A Quantum Dot Near-Field Thermophotovoltaic Device:

Created for validation of further efforts

David G. Zagyvai
Budapest University of Technology and Economics

March 26, 2025

Abstract

In the following document, an early-stage assessment can be found, with the aim to determine whether further efforts into the topic outlined in the title should be made, or not.

In this sentiment, first a clear definition of the issue to be solved is provided, followed by the theoretical outline of the quantum dot (QD) infused near-field thermophotovoltaic (NFTPV) device, the efficiency of which is calculated afterwards. Then, the concept is evaluated from an industrial and economical perspective, first describing potential means of manufacturing, including their costs, and then that is evaluated as if the investment into the technology would be profitable or not.

These being said, the intention of this paper should be clear, and is as summarized: *To provide the proof of principle for a market-ready heat-to-electricity conversion device.*

Problem definition

As of 2024, countless efforts have been made to mitigate the harmful effects of climate change and to provide abundant sources of energy. [1] [32] [3] For a prosperous future, humanity has to adapt to the challenges that try to diminish these efforts, given that sustainably sourced energy is a necessity for nearly all fields of endeavors. Not only is this crucial, but also to find solutions, that can be implemented on a large scale, while being accessible for as many people as possible.

For this reason, an energy harvesting device is investigated in this paper, which can provide the solution for the issue of lack of clean energy, while fulfilling all of the further criteria. This could be done by thermophotovoltaic technologies, which are already thoroughly investigated. [7] [23] [9] [15]

In our currently researched case, it would be done by a NFTPV, whose emitter layer would consist of a QD thin-film, thus allowing the emitted heat to fit well to the absorption spectrum of the absorbing layer. The original idea had been presented in a paper describing the near-field thermal emittance of QDs [46], and so this research aims to further develop that concept, by pairing it with a device concept and economical validation.

Device concept

The description of the device previously mentioned is the most important part of this paper, given that this concept is the basis for all further calculations. It can be described layer-by-layer, from the back to the front in the following way, and as shown in Figure 1:

- Aluminium back contact layer:

  Serving as the back contact for the photovoltaic (PV) that generates the electricity, it would only be required to be a few micrometers of thickness [26], covering the entirety of the PV cell.

- Silicon photovoltaic:

  This shall be a classical PV-cell, consisting of an N-type layer and a P-type layer. The only difference from its regular version would be that on the front-facing surface of the N-type layer, chemical etching should be performed, leaving pillars of the material [16], serving as nanogap spacers between the emitter and absorber layers. Moreover, the same surface should be oxidized before the etching and assembly procedure, to form SiO_2, which has optimal thermal conductivity to serve as a thermal insulator between the absorber and emitter layers. [25] [10] [22] This is crucial to minimize heat exchange by conduction, and thus maximize cell efficiency.

- Transparent conductive polymer (TCP):

  This layer shall be deposited onto the front facing surface of the PV, before the peeling of the photoresist required for the etching. [35] The use of this material, namely an ITO polymer, would allow the collection of charges as a front contact [5],

while also allowing photons to reach the PV from the QDs, thus allowing the near-field effects to take place without significantly deteriorating cell performance.

- QD thin-film:

  The most innovative element of the whole device is the notion to use QDs as the emitters of an NFTPV, which would capitalise on the quantum-confinement effect of QDs, while also benefiting from near-field effects.[45] This would result in a near-field thermal radiation spectrum that is highly modulated, and that can be tailored for the c-Si PV by choosing the right size for the QDs.[46]

- Aluminium sheet:

  To serve both as a surface on which the QD thin-film can be deposited and as a structural component as well, an aluminium sheet is chosen, for its great strength and thermal conductivity[21] to price ratio.

With this described device, it is assumed that a great efficiency and power output could be achieved, while maintaining cost efficiency. These are investigated hereon.

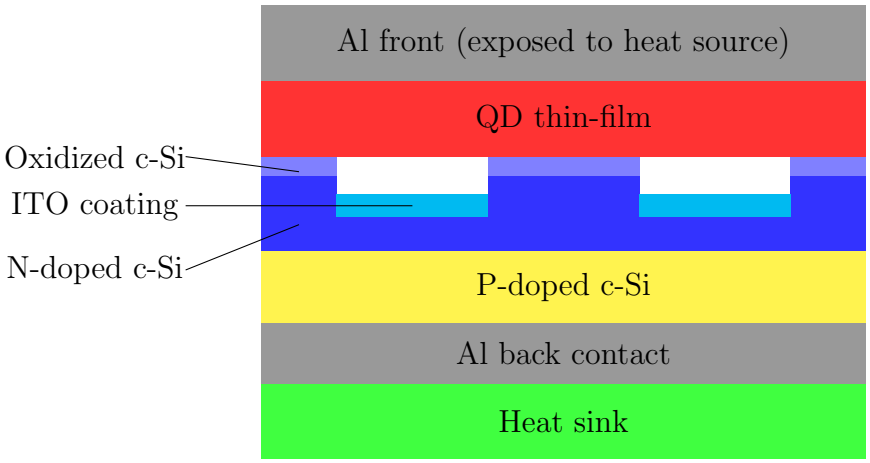

Figure 1: Schematic of the conceptual QD-NFTPV

Efficiency calculation

The efficiency of the device is one of the most important aspects of the concept when the feasibility is determined. For this reason, the described device's efficiency is calculated by comparing the efficiently absorbed radiation to the total radiation output, using the spectrum of both. It is done via the following methods.

Methodology

The following steps have been performed to determine the approximated efficiency of the device:

1. Extraction of data from literature:

   For this step, the near-field thermal radiation spectrum of QDs [46] and the external quantum efficiency (EQE) of a c-Si cell [2] is gathered via the PlotDigitizer online tool, which allows for the discrete data point extraction of curves, which were found in the listed literature.

2. Adjust units:

   Standardized units are required to allow the comparison of different photonic properties. For that purpose, the radiation spectrum, which is given as spectral Local Density of States (LDOS) as a function of wavenumber, has to be converted so that it is as a function of photon energies. This can be done using the following equation:

$$E = k * h \tag{1}$$

Where E is the energy of photons emitted, k is the wavenumber and h is the Planck's constant, which equals to $6.62607015 * 10^{-34}\ \frac{m^2 kg}{s}$. The EQE is given as a function of wavelength, but should be in E as well. It can be converted via the following equation:

$$E = \frac{h * c}{\lambda} \tag{2}$$

Where c is the speed of light, which equals to $299792458\ \frac{m}{s}$ and λ is the wavelength.

3. Convert spectral LDOS to spectral energy density:

   To turn the spectral LDOS as a function of angular frequencies into spectral energy density as a function of photon energies, it has to be converted first into spectral energy density as a function of angular frequency, then into spectral energy density as a fucntion of photon energies, which is our required final product. The first conversion is as simple as

$$u(\theta, x) = n(\theta, x) * E \tag{3}$$

   where $u(\theta, x)$ is the spectral energy density, $n(\theta, x)$ is the spectral LDOS and E is the corresponding photon energy.[30]

   To then turn these into spectral energy densities as a function of photon energies, we have to consider the equation $\theta = \frac{E}{\hbar}$, where $\hbar$ is the reduced Planck's constant and is equal to $1.054571817 * 10^{-34}\ \frac{m^2 kg}{s}$. Converting this formula into $E = \theta\hbar$, it can be seen, that the following equation gives the desired spectral energy density:

$$u(E, x) = u(\theta, x) * \frac{1}{\hbar} \tag{4}$$

$$u(E, x) = n(\theta, x) * \frac{E}{\hbar} \tag{5}$$

Using this formula on each discrete data point, it is possible to convert the graph of spectral LDOS into the appropriate spectral energy density.

4. Determine corresponding EQEs:

   As the photon energy values of the u function do not directly correspond to the ones extracted from the EQE graph, there has to be an approximation to obtain the required data points. For this purpose, a linear approximation of the EQE graph is implemented, which is used to find the appropriate EQE values for each photon energy value of the $u(E, x)$ graph. Using this method, the required EQE data points are retrieved.

5. Calculate efficiently absorbed radiation and total radiation:

   For the calculation of the efficiently absorbed spectral radiation, the following formula is implemented:

$$u_{eff}(E, x) = u(E, x) * \eta_{ext}(E) \tag{6}$$

   Where u_{eff} is the efficiently absorbed radiation and η_{ext} is the EQE. Following this calculation for each data point, the total efficiently absorbed radiation and the total radiation output is obtained by using the trapezoidal integral method, as shown in equation (7) for the former and equation (8) for the latter.

$$U_{eff}(x) = \int_0^\infty u_{eff}(E, x)dE \approx \sum_{k=1}^{k_{Emax}} (E_k - E_{k-1}) * \frac{u_{eff}(E_k) - u_{eff}(E_{k-1})}{2} \tag{7}$$

$$U(x) = \int_0^\infty u(E, x)dE \approx \sum_{k=1}^{k_{Emax}} (E_k - E_{k-1}) * \frac{u(E_k) - u(E_{k-1})}{2} \tag{8}$$

6. Calculate efficiency:

   From the previously obtained U_{eff} and U, the efficiency can be easily obtained by division of the two values:

$$\eta = \frac{U_{eff}(x)}{U(x)} \tag{9}$$

Using the aforementioned methods the theoretical efficiency of the device is calculated in Microsoft Excel. The graphs obtained during steps 1., 3. and 6. are shown in Figure 2.

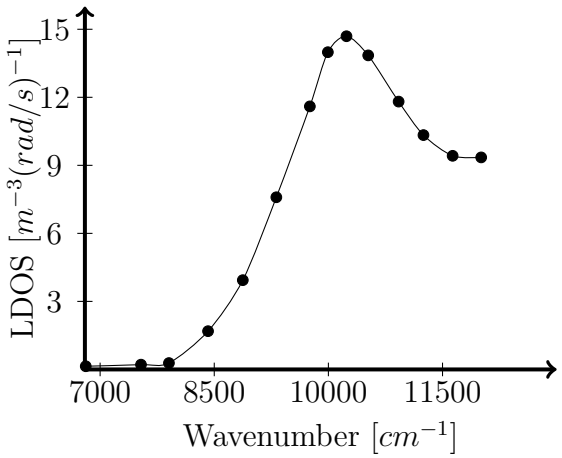

(a) Graph of the spectral LDOS emitted by PbS QDs

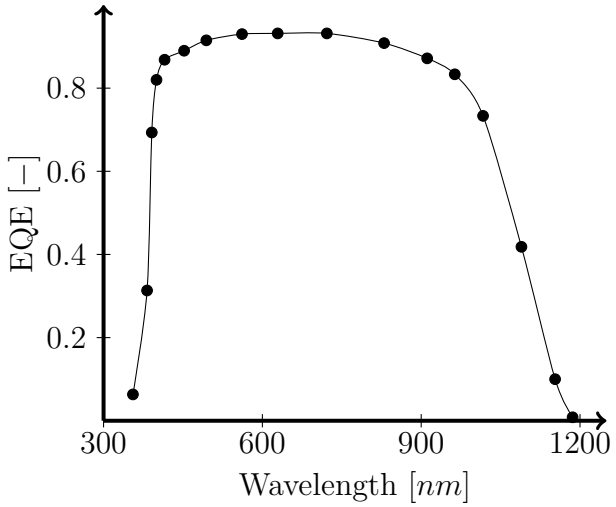

(b) Graph of EQE of c-Si solar panels

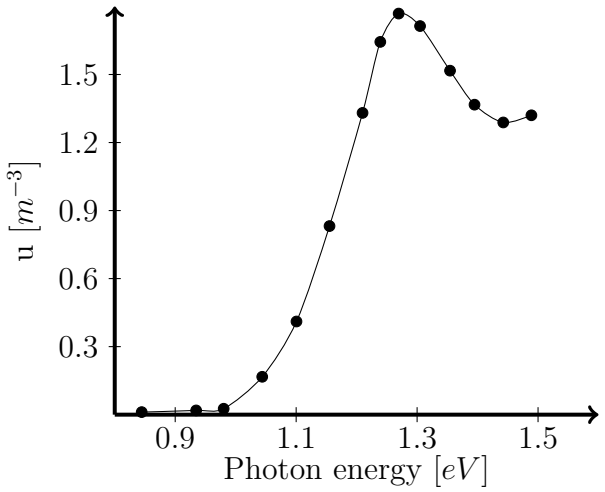

(c) Graph of spectral energy density

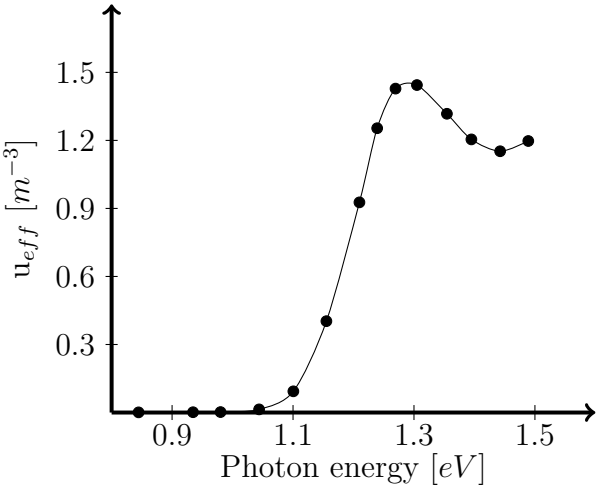

(d) Graph of efficiently absorbed spectral energy density

Figure 2: Graphs used for calculating the theoretical efficiency of the investigated device

Results

After completing the above outlined steps, a previously unseen efficiency of $\eta \approx 76\%$ is calculated. While this value by itself is not enough to draw direct conclusions without taking manufacturing costs into account, and also recognising the exclusion of factors such as heat loss by conduction and reflection losses, this is still a good indicator of the fact, that the technology holds great potential.

Manufacturing costs

Another crucial factor in validating the technology is determining the manufacturing costs. To allow these calculations, first a list of materials are produced with price per cell calculations, then the manufacturing methods are listed as well, with calculation on prices per cell for a hypothetical recoupment time.[1]

Material prices

For each of the outlined layers, a selection of materials is made based on price and quality, and based on the selected material, a cost simulation is made. As a basis for all further calculations, cell size is:

$$A_{cell} = 1\ cm^2 = 1 * 10^{-4}\ m^2 \tag{10}$$

Aluminium back contact

This layer requires an aluminium paste[41], the price of which is calculated in the following way:

Layer thickness see lit.[26] $[h] = m$	Layer volume $V = h * A_{cell}$ $[V] = m^3$	Density see lit.[41] $[\rho] = \frac{kg}{m^3}$	Mass $m = V * \rho$ $[m] = kg$	Price /kg see lit.[41] $[\frac{P}{m}] = \frac{\$}{kg}$	Price $P = m * \frac{P}{m}$ $[P] = \$$
$1 * 10^{-5}$	$1 * 10^{-9}$	2710	$2.71 * 10^{-6}$	3.98	$1.0785 * 10^{-5}$

Table 1: Cost per cell of aluminium paste back contact

As it can be seen above, the total price per cell for this element is $1.0785 * 10^{-5}$\$.

1. The sources of the material and equipment prices are from various vendors, and so while the exact prices may vary, it wouldn't significantly change the total outcome of the manufacturing cost assessment.

Doped c-Si cell

For the entirety of the c-Si cell, an N-type doped [12] and a P-type doped [13] semiconductor wafer is required. Both of their cost analysis can be seen in Table 2 and 3:

Wafer area see lit. [13] $[A_{wafer}] = m^2$	Number of cells $N = \frac{A_{wafer}}{A_{cell}}$ $[N] = -$	Price of wafer see lit. [13] $[P_{wafer}] = \$$	Price per cell $P = \frac{P_{wafer}}{N}$ $[P] = \$$
0.0441	441	1.9	$0,0043$

Table 2: Cost per cell of P-type doped c-Si wafer

Wafer area see lit. [12] $[A_{wafer}] = m^2$	Number of cells $N = \frac{A_{wafer}}{A_{cell}}$ $[N] = -$	Price of wafer see lit. [12] $[P_{wafer}] = \$$	Price per cell $P = \frac{P_{wafer}}{N}$ $[P] = \$$
0.0324	324	1.2	$0,0037$

Table 3: Cost per cell of N-type doped c-Si wafer

And so the summarized cost of the c-Si wafers per cell is $0.0043 + 0.0037 = 0.008\$$.

Transparent conductive polymer coating

The approximated cost calculation for the ITO polymer, that can be supplied in a powder form [27], is in Table 4:

Powder mass see lit. [27] $[m_p] = kg$	Thickness see lit. [5] $[h] = m$	Density see lit. [27] $[\rho] = \frac{kg}{m^3}$	Coating mass $m = \rho * h * A_{cell}$ $[m] = kg$	Price see lit. [27] $[P_p] = \$$	Price per cell $P = P_p * \frac{m}{m_p}$ $[P] = \$$
0.1	$1 * 10^{-8}$	850	$8.5 * 10^{-8}$	245	0.00021

Table 4: Cost of ITO polymer coating per cell

It can be seen, that a transparent conductive polymer coating on the etched surface of the N-type wafer would cost 0.00021$.

PbS QDs

The most important part of the device, the QD thin-film shall consist of PbS QDs of the appropriate size[33], which provide the modulation of the thermally emitted radiation. Their price is calculated in the following way:

Solution mass see lit.[24] $[m_s] = kg$	Thickness see lit.[29] $[h] = m$	Density see lit.[24] $[\rho] = \frac{kg}{m^3}$	Solution price see lit.[24] $[P_s] = \$$	Price $P = P_s * \frac{\rho * h * A_{cell}}{m_s}$ $[P] = \$$
$5 * 10^{-5}$	$1 * 10^{-8}$	1000	397.6	0.00795

Table 5: Cost per cell of QD thin-film

From Table 5, the price of the QD layer can be read: 0.0795$.

Aluminium front sheet

The other structural element of the device is a strong aluminium sheet[21], that is the layer transferring the heat to the QDs, while also serving as their base. Its price is calculated in Table 6:

Size of sheet see lit.[44] $[A_s] = m^2$	Number of cells $N = \frac{A_s}{A_{cell}}$ $[N] = -$	Price of sheet see lit.[44] $[P_s] = \$$	Price per cell $P = \frac{P_s}{N}$ $[P] = \$$
2	20000	50.47	0.0025

Table 6: Cost per cell of aluminium sheet

As of the above calculations, the price per cell of the aluminium sheet is 0.0025$.

Summarized

Now that the necessary calculations have been made and the material costs per cell are obtained, these shall be summarized to get the total cost per cell as a result. For later

comparison purposes a panel price is also calculated, where:

$$A_{panel} = 1\ m^2 \tag{11}$$

$$N_{\frac{cells}{panel}} = \frac{A_{panel}}{A_{cell}} = 10000 \tag{12}$$

With this being considered, the total costs are calculated per Table 7:

Aluminium paste	$1.0785 * 10^{-5}$\$
c-Si wafers	0.008\$
Polymer coating	0.00021\$
PbS QDs	0.00795\$
+ Aluminium sheet	0.0025\$
Total price per cell	0.01867\$
Total price per panel	186.70785\$

Table 7: Total material costs

And so the sum of the material costs is 0.01867\$ per cell and 186.70785\$ per panel.

Procedural costs

To calculate the cost of manufacturing procedures, the following steps are assumed:

1. Oxidization of a surface of N-type silicon wafer [25] [10] [22];
2. Bonding of the same wafer with its P-type counterpart [19] [38];
3. Etching the oxidize surface to form SiO_2 nanopillars [16] [31] [6];
4. Apply ITO polymer coating to etched surface, either via spin coating, screen printing or other manufacturing methods [4] [28], then remove photoresist used for etching, thus also removing excess TCP from the spacer pillars;
5. Apply aluminium paste to the other side of the wafer via screen printing to form the back contact [26];

6. Apply QD thin-film onto an aluminium sheet via screen printing, spin coating, or other methods [34] [43] [42] [29];
7. Assemble the emitter and absorber parts, creating the final device [18].

These steps altogether require the equipment listed below:

- Annealing furnace for step 1.;
- Bonding chamber for step 2.;
- Etching machine for step 3.;
- Screen printer for steps 4., 5. (and 6.);
- Possibly a spin coater for step 6.;
- Glove box for step 7.

The price of these pieces of equipment are calculated per cell by assuming recoupment time $T = 5\ years$, a number of purchases per annum of $N = 200\ \frac{orders}{year}$, with an area of each order as $A = 10\ m^2$. From these, the total number of cells, N_{total}, from which the price of the machinery shall be recouped is calculated in the following way:

$$N_{total} = T * N * \frac{A}{A_{cell}} = 10^8 \tag{13}$$

This means, that each cost of the machines shall only be added after a division of N_{total}, which yields the desired price per cell of them.

Following that, the cost of each machine is listed below, with price per cell calculation, which than a price per panel calculation follows.

Annealing furnace [17]	30000$
Bonding chamber [20]	5000$
Etching machine [8]	4000$
Screen printer [36]	5000$
Spin coater [39]	4500$
Glove box [14]	5000$
Total price	53500$
Total price per cell	0.000535$
Total price per panel	5.35$

Table 8: Total price of manufacturing equipment

Labor cost

Without deeper research conducted in the field of human resources, a general multiplier of 0.5 is applied to all material costs. This surely is a drastic approximation, but considering the uncertain nature of labor costs, it would be nearly impossible to give a significantly more accurate estimate.

Total cost summary

With all of the previously listed costs, it can be summed as in Table 9:

Item	Price per cell	Price per panel
Material cost	0.01867$	186.70785$
Labor cost	0.009335$	93.353925$
Equipment cost	0.000535$	5.35$
Total	0.02854$	285.411775$

Table 9: Total manufacturing cost summary

And so the total prices come down to 0.029$ per cell and 285.41$ per panel.

Economical evaluation

Now that the efficiency and the costs have been calculated, it is possible to compare it to different technologies, and decide whether it is an economically valid concept or not.

Firstly, it has to be determined where the technology can be used. There are areas, where it could replace already existing solutions [33], but its unique ability to efficiently convert heat into electricity would also allow for previously unattainable areas of usage. An example for both is given in this section of the paper.

Solar alternative

The first of the two aforementioned examples is a solar application. In this configuration, the technology would be used to convert heat collected from solar rays into electricity at a high efficiency. To compare its efficiency, we shall assume that the efficiency that is lost because the NFTPV would radiate heat outwards as well, would not exceed 20%, which is the basic radiative heat loss for regular PV cells. However, it should be noted, that with further research and development, it could be possibly further reduced. After clearifying this, an efficiency of $\eta_{total} = \eta * 0.8 = 61\%$ is considered.

The PV panel's important specifications that we use for comparison [37] and our NFTPV panel's specifications are listed in Table 10.

Device	Panel size	Efficiency	Cost
Regular PV	0.77 m^2	21%	110$
NFTPV	1 m^2	61%	294$

Table 10: Technical specification of compared solar technologies

From this data, it is visible that an $\alpha = \frac{Price}{Efficiency * Area}$ ratio for the regular PV is $\alpha_{PV} = 680\ \frac{\$}{1*m^2}$, while it is $\alpha_{NFTPV} = 482\ \frac{\$}{1*m^2}$ for the QD-NFTPV. This means, that as

efficiency is linearly proportionate to power output, this α ratio will represent how much would a system of the same power output cost. As for the NFTPV, this is much lower than for the regular PV, which indicates that the usage of the former technology would not only be more effective at places with less surface area, but would also be more cost-effective. Thus the application as a solar cell alternative seems to hold potential.

Data center cooling

Countless areas can be found, where cooling is a necessity, and an example of these is becoming more and more important daily: data center cooling [11]. As there is no existing solution on how to effectively recycle waste heat in this scenario, the technology in question could create a market of its own in this particular area. Yet, it still has to be determined how quick an investment in this field would recoup over time.

To do so, a typical server rack is assumed, with dimensions of 1900 mm x 1100 mm x 650 mm, and with a maximum power output of 8 kWs [40]. These specifications allow for the calculation of a hypothetical energy, and so cost saving per rack. To cover the entire surface, it would cost $A_{rack} * \frac{Price}{Panel} \approx 2380\$$. The savings can be calculated by $P_{rack} * T_{\frac{hours}{year}} * \eta * \frac{Price}{kWh} \approx 9214 \frac{\$}{year}$. This shows, that the investment into this technology at data centers would recoup in a mere 3 months, also proving this application to be economically feasible.

Conclusion and recommendation

After the previous calculations, the study shows, that the use of a quantum dot thin-film for the emitter region of a near-field thermophotovoltaic device theoretically can be done to raise the efficiency of previously tested devices. Not only could it achieve an unprecedented heat-to-electricity conversion efficiency of 76%, but it would also do so at a competitive price, which was first calculated by considering the costs of the materials used, the cost of labor, and the cost of manufacturing equipment, and then was evaluated by comparison and by calculating the effects of possible investment as well. As it is now shown to be theoretically possible, the principle is considered to be proved.

The idea now has to be tested experimentally to gain exact measurements, and after that, several areas are open for investigation in the field of heat-to-electricity conversion. And so the aim of the paper is successfully reached: *The technology is shown to hold potential and based on the description of the device, experimental research can be carried out.*

References

[1] Joseph E Aldy, Richard Baron, and Laurence Tubiana. Addressing cost: The political economy of climate change. *Beyond Kyoto: Advancing the international effort against climate change*, pages 85–110, 2003.

[2] Wisnu Ananda. External quantum efficiency measurement of solar cell. In *2017 15th International Conference on Quality in Research (QiR) : International Symposium on Electrical and Computer Engineering*, pages 450–456, 2017.

[3] Daniel Bodansky. Climate commitments: assessing the options. *Beyond Kyoto: Advancing the international effort against climate change*, pages 37–60, 2003.

[4] Lakshmana Kumar Bommineedi, Nakul Upadhyay, and Rafael Minnes. Screen printing: an ease thin film technique. In *Simple Chemical Methods for Thin Film Deposition: Synthesis and Applications*, pages 449–507. Springer, 2023.

[5] Ganesh T. Chavan, Youngkuk Kim, Muhammad Quddamah Khokhar, Shahzada Qamar Hussain, Eun-Chel Cho, Junsin Yi, Zubair Ahmad, Pitcheri Rosaiah, and Chan-Wook Jeon. A brief review of transparent conducting oxides (tco): The influence of different deposition techniques on the efficiency of solar cells. *Nanomaterials*, 13(7), 2023.

[6] B Dev Choudhury, R Casquel, María José Bañuls, FJ Sanza, MF Laguna, M Holgado, Rosa Puchades, A Maquieira, CA Barrios, and Srinivasan Anand. Silicon nanopillar arrays with sio 2 overlayer for biosensing application. *Optical Materials Express*, 4(7):1345–1354, 2014.

[7] Donald Chubb. *Fundamentals of thermophotovoltaic energy conversion*. Elsevier, 2007.

[8] Beijing Golden Eagle Electronic Equipment Co. High precision chemical etching machine, 2024. Accessed on March 26, 2025.

[9] Alejandro Datas and Rodolphe Vaillon. Thermophotovoltaic energy conversion. In *Ultra-High Temperature Thermal Energy Storage, Transfer and Conversion*, pages 285–308. Elsevier, 2021.

[10] Bruce E Deal and AS Grove. General relationship for the thermal oxidation of silicon. *Journal of applied physics*, 36(12):3770–3778, 1965.

[11] Khosrow Ebrahimi, Gerard F. Jones, and Amy S. Fleischer. A review of data center cooling technology, operating conditions and the corresponding low-grade waste heat recovery opportunities. *Renewable and Sustainable Energy Reviews*, 31:622–638, 2014.

[12] Zheijang Dongshuo New Energy. 182mm*182mm m10 n type monocrystalline silicon solar wafer for solar cell, 2024. Accessed on March 26, 2025.

[13] Zheijang Dongshuo New Energy. 210mm*210mm p type monocrystalline solar silicon wafer for solar cell, 2024. Accessed on March 26, 2025.

[14] EquipX. Labconco glove box with hepa filters cat.no. 5220200, 2024. Accessed on March 26, 2025.

[15] Claudio Ferrari, Francesco Melino, Michele Pinelli, and Pier Ruggero Spina. Thermophotovoltaic energy conversion: Analytical aspects, prototypes and experiences. *Applied Energy*, 113:1717–1730, 2014.

[16] Andreas Frommhold, Alex Robinson, and Edward Tarte. High aspect ratio silicon and polyimide nanopillars by combination of nanosphere lithography and intermediate mask pattern transfer. *Microelectronic Engineering*, 99:43–49, 11 2012.

[17] APS Induction Furnace. Vacuum heat treatment electric lab furnace with water cooling system, factory price list, vacuum sintering/brazing/annealing furnace, 2024. Accessed on March 26, 2025.

[18] GJ Gajda and WH Weinberg. Glove-box-based fabrication system for inelastic electron tunneling junctions. *Review of scientific instruments*, 57(7):1388–1395, 1986.

[19] U Gösele and Q-Y Tong. Semiconductor wafer bonding. *Annual review of materials science*, 28(1):215–241, 1998.

[20] EV Group. Automated production wafer bonding system, 2024. Accessed on March 26, 2025.

[21] J Hirsch. Aluminium sheet fabrication and processing. In *fundamentals of aluminium metallurgy*, pages 719–746. Elsevier, 2011.

[22] Eugene A Irene. Models for the oxidation of silicon. *Critical Reviews in Solid State and Material Sciences*, 14(2):175–223, 1988.

[23] Marine Laroche, Rémi Carminati, and J-J Greffet. Near-field thermophotovoltaic energy conversion. *Journal of applied physics*, 100(6), 2006.

[24] Nano Optical Materials. Longer near infrared pbs/cds core/shell quantum dots – organic soluble, 2024. Accessed on March 26, 2025.

[25] NF Mott, S Rigo, F Rochet, and AM Stoneham. Oxidation of silicon. *Philosophical Magazine B*, 60(2):189–212, 1989.

[26] Fredrick Madaraka Mwema, Oluseyi Philip Oladijo, Stephen A Akinlabi, and Esther Titilayo Akinlabi. Properties of physically deposited thin aluminium film coatings: A review. *Journal of alloys and compounds*, 747:306–323, 2018.

[27] Nanografi. Indium tin oxide (ito) nanopowder/nanoparticles, 90:10, purity: 99.99 Accessed on March 26, 2025.

[28] Fernande Fotsa Ngaffo, Anna Paola Caricato, Andrea Fazzi, Manuel Fernandez, Sandro Lattante, Maurizio Martino, and Francesco Romano. Deposition of ito films on sio2 substrates. *Applied Surface Science*, 248(1-4):428–432, 2005.

[29] Ossila. Spin coating: Complete guide to theory and techniques, 2024. Accessed on March 26, 2025.

[30] Annika Ott, Zhenghua An, Achim Kittel, and Svend-Age Biehs. Thermal near-field energy density and ldos in topological 1d ssh chains and 2d ssh lattices of plasmonic nanoparticles. *arXiv preprint arXiv:2109.03073*, 2021.

[31] Yi-Hao Pai, Fan-Shuen Meng, Chun-Jung Lin, Hao-Chung Kuo, Shih-Hsin Hsu, Yia-Chung Chang, and Gong-Ru Lin. Aspect-ratio-dependent ultra-low reflection and luminescence of dry-etched si nanopillars on si substrate. *Nanotechnology*, 20(3):035303, 2008.

[32] Jonathan Pershing and Fernando Tudela. A long-term target. *Beyond Kyoto Advancing the international effort against climate change*, 2003.

[33] Nicole A. Pfiester and Thomas E. Vandervelde. Selective emitters for thermophotovoltaic applications. *physica status solidi (a)*, 214(1):1600410, 2017.

[34] Xiaodong Pi, Qing Li, Dongsheng Li, and Deren Yang. Spin-coating silicon-quantum-dot ink to improve solar cell efficiency. *Solar Energy Materials and Solar Cells*, 95(10):2941–2945, 2011.

[35] F Schue and L Giral. Photosensitive resists used in microlithography. In *Makromolekulare Chemie. Macromolecular Symposia*, volume 24, pages 21–39. Wiley Online Library, 1989.

[36] ScreenPrinting.com. Riley hopkins 300 4 color 4 station press with xyz micro registration, 2024. Accessed on March 26, 2025.

[37] SHARP. Sharp nu-ah370, 2024. Accessed on March 26, 2025.

[38] R. Stengl, T. Tan, and U. Gösele. A model for the silicon wafer bonding process. *Japanese Journal of Applied Physics*, 28(10R):1735, oct 1989.

[39] MSE Supplies. Benchtop high-speed spin coater (max. 120mm dia., 10,000 rpm) with vacuum pump &3 vacuum chucks, 2024. Accessed on March 26, 2025.

[40] Enconnex Team. Exploring server rack sizes & dimensions: Depth, width, & height, 2021.

[41] Hefei Gee-U Lift Tech. Screen printing material leaf aluminum paste aluminum pigment. Accessed on March 26, 2025.

[42] MD Tyona. A comprehensive study of spin coating as a thin film deposition technique and spin coating equipment. *Advances in materials Research*, 2(4):181, 2013.

[43] MD Tyona. A theoritical study on spin coating technique. *Advances in materials Research*, 2(4):195, 2013.

[44] Aluminium Warehouse. 2000mm x 1000mm x 1.0mm - 1050 aluminium sheet, 2024. Accessed on March 26, 2025.

[45] Saman Zare. *Engineering the Spectrum of Near-Field Thermal Radiation*. The University of Maine, 2022.

[46] Saman Zare and Sheila Edalatpour. The quantum confinement effect on the spectrum of near-field thermal radiation by quantum dots. *Journal of Applied Physics*, 130(1), 2021.